NUMERICAL SIMULATIONS OF OVEREXPANDED JETS AT A MACH NUMBER OF 3.1 IMPINGING ON A PLATE WITH AND WITHOUT A HOLE

Mathieu Varé **Christophe Bogey**
Univ Lyon, École Centrale de Lyon, INSA Lyon, Université Claude Bernard Lyon I, CNRS
Laboratoire de Mécanique des Fluides et d'Acoustique, UMR 5509
F-69134 Ecully, France
mathieu.vare@ec-lyon.fr, christophe.bogey@ec-lyon.fr

ABSTRACT

Six overexpanded jets at an exit Mach number of 3.1 and a Reynolds number of 2×10^5 have been computed by Large-Eddy Simulations (LES). The static pressure and temperature at the nozzle exit are respectively equal to 0.63×10^5 Pa and 738 K. One jet is free, and the five other ones impinge on a plate located at a distance of $L = 30r_0$, where $r_0 = D/2$ is the nozzle radius. Four plates have a hole of diameter $h = 1.33D$, $2D$, $3D$ and $4D$ whereas the fifth one has no hole, in order to study the effects of the hole on the jet flow and acoustic fields. In the downstream direction, the acoustic field is dominated by the radiation of Mach waves for all jets. In the upstream direction, the acoustic levels for the impinging jets are significatively higher than for the free jet. They are caused by sound waves generated by the impingement of the jet turbulent structures on the plate, namely the impingement noise, and reflections of Mach waves on the plate. Furthermore, the upstream sound pressure levels are highest for the plate with no hole and are reduced when the hole diameter increases, suggesting that the impingement noise is the main acoustic contribution.

1. INTRODUCTION

During a rocket launching, the hot supersonic gas jets of the engines impinge on the ground. A trench is dug under the rocket to canalize those gases. The impingement of the jets on the trench edges generates intense acoustic waves. Those waves then propagate upstream to the fairing, where they can excite the rocket structure and damage the payload. The understanding of noise generation during a rocket lift-off is thus a concern for the aerospace industry. In order to examine this problem, a simplified geometry of a rocket launching can be considered, namely a jet impinging on a plate with a hole.

Such a configuration has been investigated numerically for hot overexpanded supersonic jets, typical of rocket jets. In particular, Kawai *et al.* [1] studied the impingement of an overexpanded jet at an exit Mach number of 3.66 on a plate with a hole using an axisymmetric Large-Eddy Simulation (LES). They observed a strong acoustic radiation in the upstream direction, which they identified as the reflections of the jet Mach waves on the plate. A similar set-up has then been analyzed in the numerical work of Tsutsumi *et al.* [2] for a jet at an exit Mach number of 3.7. This work highlighted an other significant noise component in the upstream direction, generated by the impingement of the jet turbulent structures on the hole edges. Nevertheless, the dominant contribution between the two upstream components, the impingement noise and the reflections of the Mach waves, has not been clearly determined yet.

In the present work, the LES of six overexpanded supersonic jets are performed in order to identify the main component of the upstream acoustic radiation. The jets are at an exit Mach number M_e of 3.1 and a Reynolds number Re_D of 2×10^5. One jet is free while the five others impinge on a plate located at a distance L of $30r_0$ from the nozzle exit, with r_0 the nozzle radius. One plate has no hole whereas the four others have a hole of diameter $h = 1.33D$, $2D$, $3D$ and $4D$ with $D = 2r_0$, with the aim of examining the effects of the hole diameter on the flow and acoustic fields.

The paper is organized as follows. The jet parameters and numerical methods used in the LES are documented in section 2. Snapshots of the flow and acoustic fields are presented in section 3. The mean flow field is described in section 4. The acoustic fields are analyzed in section 5. Finally, concluding remarks are given in section 6.

2. PARAMETERS

2.1 Jet parameters

The six jets simulated have an exhaust Mach number $M_e = u_e/c_e$ of 3.1 and a Reynolds number $Re_D = u_e D/\nu_e$ of 2×10^5, where u_e is the exhaust velocity, c_e is the sound celerity in the jet and ν_e is the kinematic viscosity at the nozzle exit. The exhaust temperature T_e is 738K and the exhaust pressure p_e is $0.63p_0$, where $p_0 = 10^5$ Pa is the ambient pressure. One jet, labelled as M31, is free. A second one, named M31h0, impinges on a plate without a hole. The four final ones, referred to as M31h13, M31h2, M31h3 and M31h4, impinge on a plate with a hole of diameter $h = 1.33D$, $2D$, $3D$ and $4D$, respectively. For the impinging jets, the nozzle-to-plate distance L is equal to $30r_0$. The width of the plates with a

hole is r_0. The ejection parameters of the jets, the nozzle-to-plate distance and the two hole diameters $h = 1.33D$ and $2D$ are the same as those in experiments lead by CNES at the MARTEL facility and in the numerical simulations of Troyes *et al.* [3]. The six jets exhaust from a cylindrical nozzle of length $2r_0$, at the inlet of which Blasius boundary layer profiles with a thickness δ of $0.15r_0$ are imposed. Vortex rings non-correlated in the azimuthal direction are added in the boundary-layer at $z = -r_0$ to trigger the boundary layer transition from a laminar to a turbulent state, as proposed in Bogey *et al.* [4]. The mean velocity radial profiles at the nozzle exit are represented in Fig. 1(a). They are the same for all jets and they deviate from the profiles imposed at the nozzle inlet. Near the nozzle exit, the boundary layer is slightly detached from the wall due to the jets overexpansion, which explains the differences between the nozzle-exit profiles and the profiles imposed at the inlet. The radial variations of the root-mean-squared value of axial velocity fluctuations thus obtained at the nozzle exit are plotted in Fig. 1(b). In all cases, the fluctuations present a peak around $r = 0.9r_0$. The intensities of the peaks are between 1% and 1.5% of the exit velocity for all jets, indicating a similar turbulent intensity level of the shear layer at the nozzle exit.

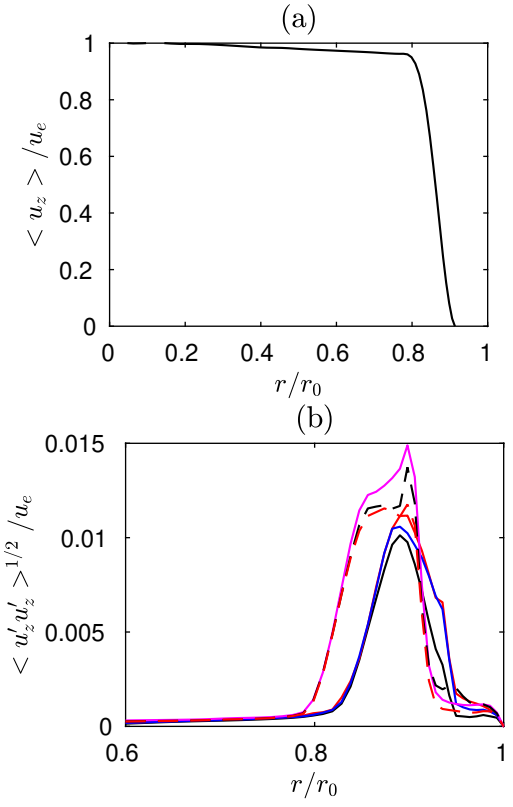

Figure 1. Nozzle-exit radial profiles of (a) mean axial velocity $\langle u_z \rangle / u_e$ and (b) axial turbulence intensity $\langle u_z' u_z' \rangle^{1/2} / u_e$: — M31h0, — M31h13, — M31h2, - - - M31h3, - - - M31h4 and — M31.

2.2 Numerical parameters

In the simulations, the unsteady compressible Navier-Stokes equations in cylindrical coordinates (r, θ, z) are solved using an OpenMP based in-house solver. The time integration is performed using a six-stage Runge-Kutta algorithm [5] and the spatial derivatives are evaluated with eleven-point low-dispersion finite-difference schemes [6]. At the end of each time step, a selective filtering is applied to remove grid-to-grid oscillations [5]. This filter dissipates kinetic turbulent energy near the grid cut-off frequency, thus acting as a subgrid-scale model. Solid and adiabatic wall conditions are implemented at the plate and nozzle walls. To handle shock waves, a damping procedure using a dilatation-based shock detector and an optimized filter are used to remove Gibbs oscillations in the vicinity of shocks [7]. The radiation boundary conditions of Tam & Dong [8] are imposed to the radial and lateral boundaries of the computational domain. They are used in combination with sponge zones using grid stretching and Laplacian filtering to prevent significant spurious reflections [9]. The method of Mohseni & Colonius [10] is applied to remove the singularity on the jet axis. The first point close to the axis is located at $r = \Delta r/2$, where Δr is the radial mesh size. The effective azimuthal resolution near the origin of the polar coordinates is reduced down to $2\pi/16$ to increase the time step of the simulation [11].

2.3 Computational parameters

The parameters of the mesh grids used in the simulations are provided in Tab. 1. In the six simulations, the numbers of points in the radial and azimuthal directions are 501 and 256, respectively. In the axial direction, the numbers of points are equal to 2628 for M31, to 1910 for M31h0 and to 2950 for M31h13, M31h2, M31h3 and M31h4. The grids thus contain between 250 and 380 millions of points. They extend out to $r = 15r_0$ in the radial direction. In the axial direction direction, they extend down to $z = 30r_0$ for the plate with no hole and down to $z = 50r_0$ for the other cases. The variations of the radial mesh spacing are presented in Fig. 2(a). It is equal to $\Delta r = 0.025r_0$ on the axis and progressively decreases down to $\Delta r = 0.0072r_0$ in the shear layer, at $r = r_0$. It then increases to reach $\Delta r = 0.05r_0$, which allows to have a Strouhal cut-off number $St = fD/u_e$ of 2.03 for an acoustic wave discretized with 5 points per wavelength, where f is the frequency of the wave. The axial mesh spacing is plotted on Fig.2(b). It reaches a minimum value of $\Delta z = 0.014r_0$ at the nozzle exit. For the free jet, it increases up to $\Delta z = 0.03r_0$ at $z = 50r_0$. For the impinging jets, the axial mesh spacing is stretched until it attains $\Delta z = 0.022r_0$ from $z = 20r_0$ to $z = 25r_0$. It is then reduced to reach again its minimum value on the plate at $z = 30r_0$, as in recent simulations of subsonic jets impinging on a plate with a hole [12]. For the plates with a hole, the axial mesh size increases after the plate up to $\Delta z = 0.03r_0$ at $z = 50r_0$. The extrema values of the mesh spacings and the elongation rates in radial and axial directions are the same as those in the simulations of jets at a Mach number

	n_r	n_θ	n_z	$n_r \times n_\theta \times n_z$
M31	501	256	2628	340 $\times 10^6$
M31h0	501	256	1910	250 $\times 10^6$
M31h13, M31h2, M31h3, M31h4	501	256	2950	380 $\times 10^6$

Table 1. Mesh parameters: numbers of points n_r, n_θ and n_z in the radial, azimuthal and axial directions, and total numbers of points.

of $M = 2$ of Pineau & Bogey [13]. The results presented in this work have been obtained after simulation times of $1000 r_0/u_e$ for all jets.

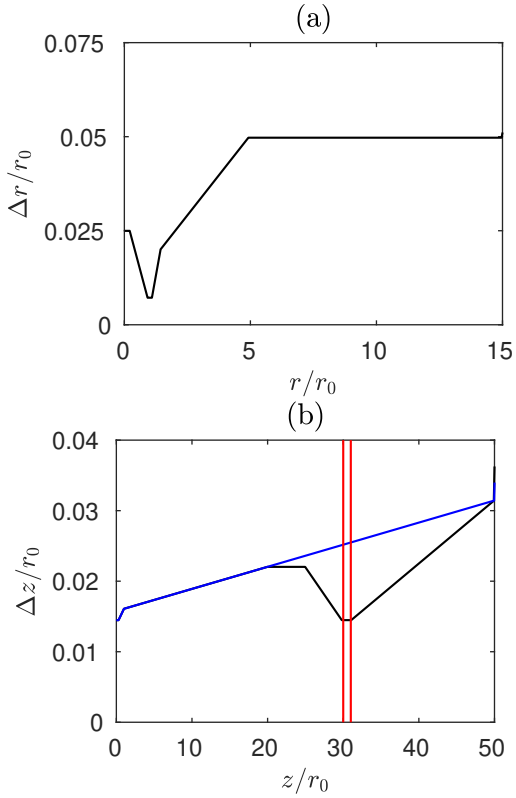

Figure 2. Variations of (a) radial and (b) axial mesh spacings: — impinging jets, — free jet, — positions of the upstream and downstream faces of the plate.

3. SNAPSHOTS OF THE FLOW AND ACOUSTIC FIELDS

Snapshots of the jet flow and acoustic fields are shown in Fig. 3. Fluctuations of temperature are represented inside the flow and fluctuations of pressure outside. For the six jets, diamond patterns characteristic of shock cells are visible at the nozzle exit. Two shock cells are observed in the jets until the cell pattern is progressively weakened by the turbulent mixing. For the impinging jets represented in Fig. 3(a) to 3(c), a wall jet is created by the impingement of the flow on the plate. The wall jet is most developed for the plate with no hole and is less apparent when the hole diameter increases.

The acoustic radiation of the jets can be seen in the pressure fields of Fig. 3. For the free jet in Fig. 3(f), acoustic waves of weak amplitude propagate upstream. This upstream radiation corresponds to the broadband shock-associated noise (BBSAN), produced by the interactions between the turbulent structures of the mixing layers and the shock cells. In the downstream direction, inclined wavefronts of strong amplitude are visible in the sound field, which is typical of Mach wave radiation, as observed for instance in the simulations of a jet at $M_e = 3.3$ by De Cacqueray *et al.* [14]. These waves are produced by the convection of turbulent coherent structures at a supersonic speed. The Mach angle α between the direction of propagation of the Mach waves and the jet axis can be evaluated with the relation

$$\alpha = \cos^{-1}\left(\frac{c_0}{u_c}\right) = 68^o \qquad (1)$$

where u_c is the convection velocity of the turbulent structures of the jet, estimated here by $u_c = 0.54 u_e$, and c_0 is the ambient sound velocity. The angle given by Eq.(1) is in agreement with the direction of propagation of the Mach waves observed in Fig. 3(f). Similar Mach waves are present in the pressure fields of the impinging jets in Fig. 3(a) to 3(e). Moreover, strong spherical acoustic waves propagate in the upstream direction for these five cases. Their levels are significatively higher than those of the upstream sound waves generated by the free jet. Those levels are the highest for M31h0 and are the weakest for M31h4, suggesting that they are due to the impingement noise. For the plates with a hole in Fig. 3(b) to 3(e), the sound field downstream of the plate has no clear organization, even if acoustic waves seem to originate from the hole.

4. PROPERTIES OF THE MEAN FLOW FIELDS

The variations of the centerline mean axial velocity are plotted on Fig.4. For the six jets, the velocity does not deviate too much from the exhaust velocity down to $z = 16 r_0$, which corresponds to the end of the potential core defined by an axis velocity of $0.9 u_e$. Accelerations and decelerations are visible. They are linked to the shock cells. Six shock cells are found in the mean axial velocity profiles and they are progressively dampened by the turbulent mixing. The location and the amplitude of the shocks is the same for all jets. The first cell length L_s is evaluated at $L_s = 4.6 r_0$. For the free jet, the velocity decreases after the end of the shock cell patterns. The sonic core, defined by an axis velocity equal to c_e, closes around $z = 40 r_0$.

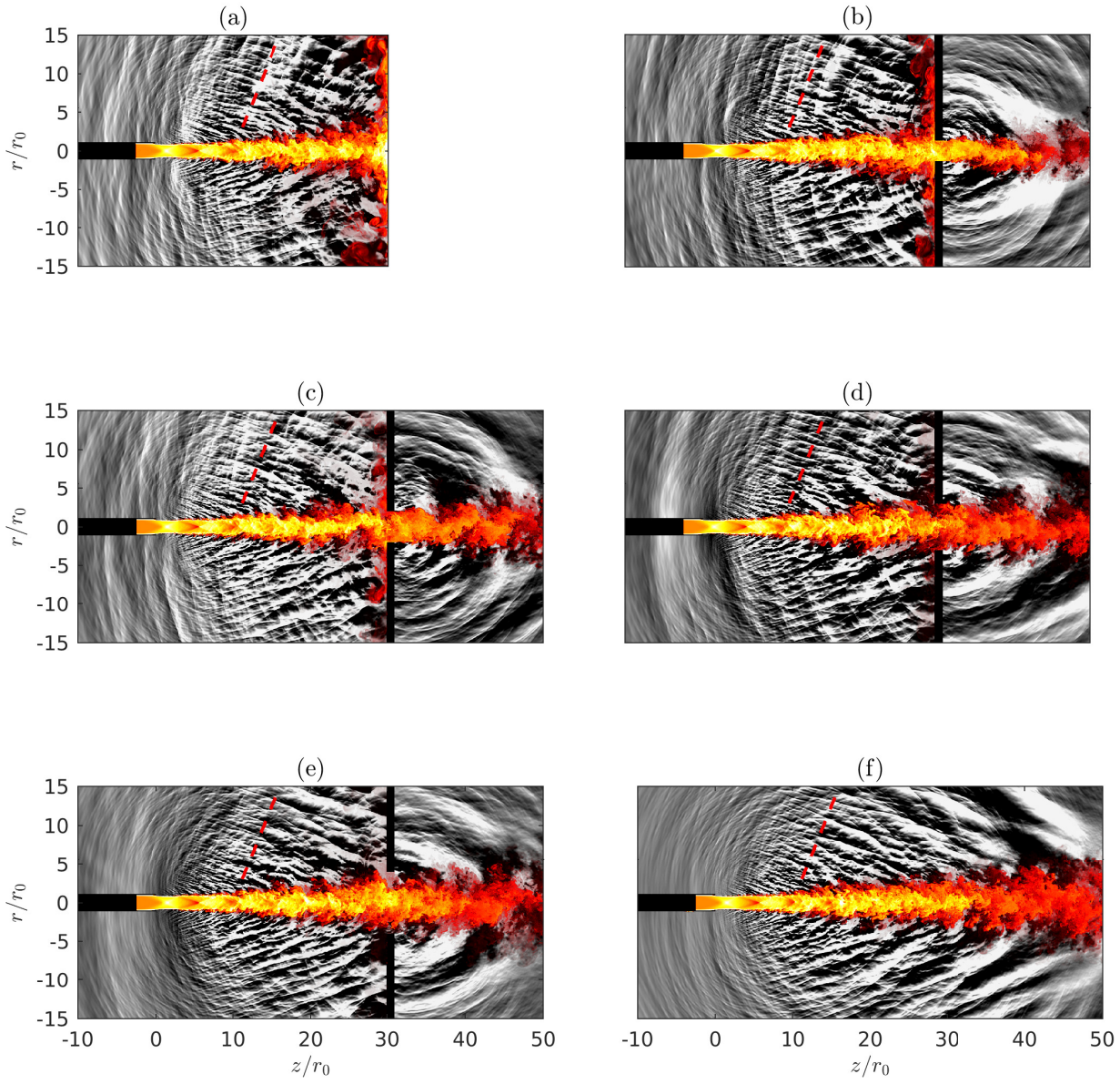

Figure 3. Snapshots in the (z, r) plane of the fluctuations of temperature in the flow and of pressure outside for (a) M31h0, (b) M31h13, (c) M31h2, (d) M31h3, (e) M31h4 and (f) M31. The color scales range from 0 to 780K for the temperature and from -2000 to 2000 Pa for the pressure. The dashed line - - - indicates the direction $\alpha = 68°$ with respect to the jet axis.

In the case of the plate with no hole, the velocity declines abruptly from $z = 28r_0$ down to the plate. For the plates with a hole, the variations of velocity are similar to those for the free jet. In particular, the sonic core closes after the plate, around $z = 40r_0$, which is in agreement with the simulations of Troyes *et al.* [3]. Therefore, the plate with a hole has a weak effect on the mean axial velocity.

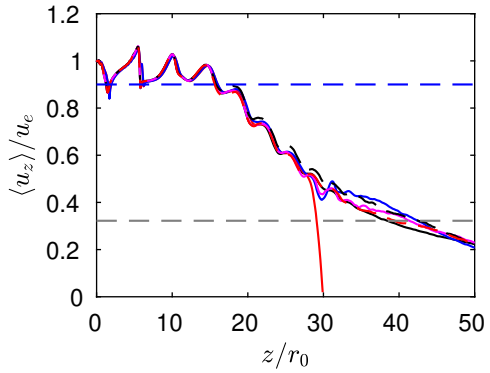

Figure 4. Variations of the mean axial centerline velocity $\langle u_z \rangle / u_e$ for — M31, — M31h0, — M31h13, — M31h2, - - - M31h3 and - - - M31h4; - - - $0.9u_j$ and - - - c_e.

5. PROPERTIES OF THE ACOUSTIC FIELDS

5.1 Pressure spectra near the nozzle

The acoustic spectra at $r = 2r_0$ and $z = 0$ near the nozzle are shown in Fig.5. For the free jet, a bump is located at $St = 0.06$ in the pressure spectrum. This frequency is compared with the central frequency f_p of BBSAN estimated by the model of Harper-Bourne & Fisher [15]

$$f_p = \frac{u_c}{L_s(1 - M_c \cos\theta)} \tag{2}$$

with $M_c = u_c/c_0$ the convection Mach number and θ the angle between the jet axis and the far-field observation point. The upstream direction $\theta = 180^o$ is considered here. The relation (2) gives a Strouhal number of $St_p = 0.068$, which is close to the frequency of the bump in the spectrum of the free jet. For M31h0, the levels are about 12 dB higher than those for the free jet. A large peak is found around $St = 0.04$ in the acoustic spectrum. For the plates with a hole, the levels decrease as the hole diameter increases. With respect to M31h0, the noise reduction is approximately of 3 dB for M31h13, 4 dB for M31h2, 8 dB for M31h3 and 10 dB for M31h4. This noise reduction suggests that the interactions between the jet and the hole edges are less strong for larger holes, leading to a diminution of the impingement noise. For M31h13 and M31h2, compared with the case with a full plate, the pressure levels are only reduced for $St \geq 0.1$. For M31h3, a diminution of the levels is noticed for all frequencies relative to M31h2. Finally, for M31h4, the acoustic levels decrease only for $St \leq 0.2$ with respect to M31h3.

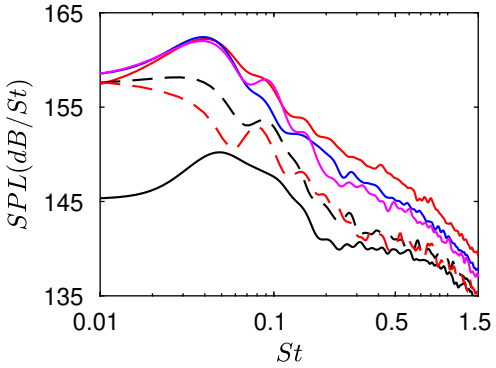

Figure 5. Sound pressure levels (SPL) at $z = 0$ and $r = 2r_0$ as a function of the Strouhal number St for — M31h0, — M31h13, — M31h2, - - - M31h3, - - - M31h4 and — M31.

5.2 Azimuthal structure of the jets

The pressure fields of the six jets have been decomposed in their two first azimuthal modes. The contributions of these modes to the spectra at $r = 2r_0$ and $z = 0$ are shown in Fig.6. In all cases, the axisymmetric mode $n_\theta = 0$ is predominant at Strouhal numbers lower than 0.1. The acoustic levels are the highest for this range of frequencies, suggesting that the axisymmetric mode is the dominant mode of the upstream acoustic radiation. The acoustic levels associated to the axisymmetric mode decreases drastically for $St \geq 0.2$. For the six jets, the contribution of the azimuthal mode $n_\theta = 1$ is negligible for $St \leq 0.1$. For higher Strouhal numbers, it becomes more important than the contribution of the axisymmetric mode. However, at theses frequencies, the pressure levels of the two first modes are lower between 1 and 15 dB than the total level, which shows that higher order azimuthal modes are significant here. The jet impingement on the plate does not modify noticeably the azimuthal structure of the upstream acoustic field.

5.3 Far field overall sound pressure levels

The overall sound pressure levels (OASPL) at $r = 15r_0$ are plotted in Fig.7. For the free jet, they increase with the axial distance up to a maximum value of 160 dB reached at $z = 29r_0$. Then they slowly decrease to 155 dB at $z = 50r_0$. The maximum value is obtained in the downstream direction of the jet because of the directivity of the Mach waves. For the jet impinging on a plate with no hole, the OASPL also increase with the axial distance. Its maximum value of 168 dB is located at $z = 28r_0$. Nevertheless, between $z = 25r_0$ and $30r_0$, hydrodynamic pressure fluctuations of the wall jet are taken into account in the OASPL. Outside of this zone, the OASPL of M31h0 are higher between 3 and 7 dB than the levels of the free jet. For the jets impinging on a plate with a hole, the OASPL follow a similar evolution as for M31h0. They are reduced as the hole diameter increases. With respect to the case with no hole, the pressure levels are lower by approxi-

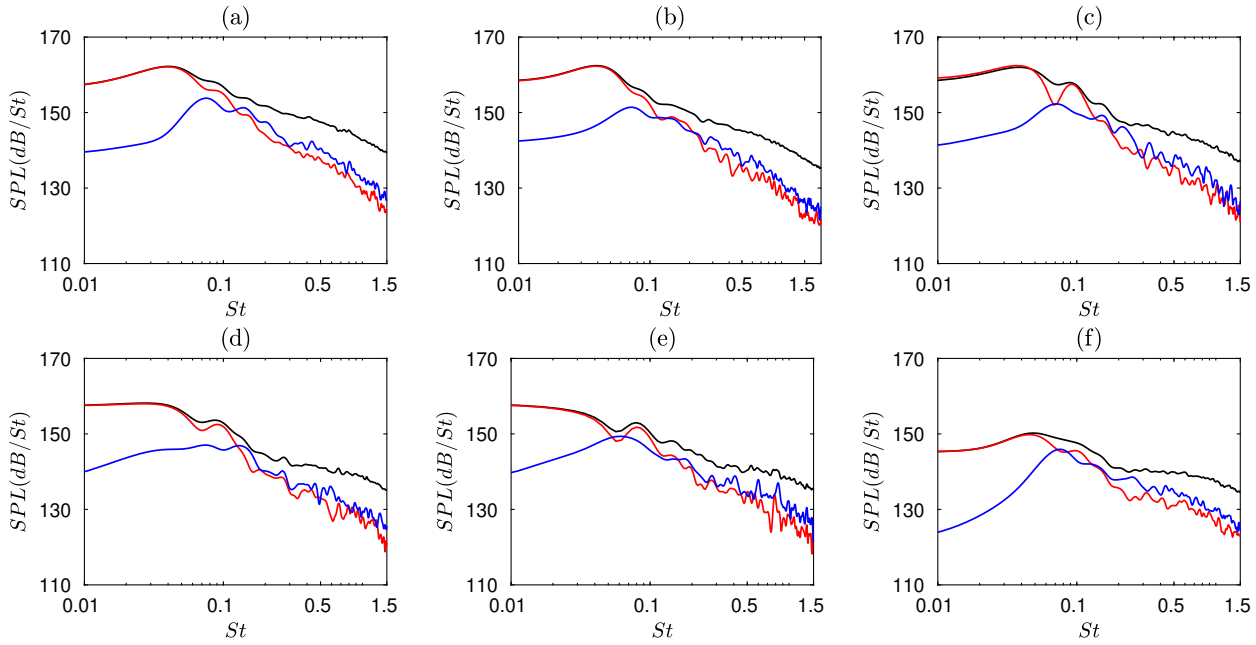

Figure 6. Acoustic spectra at $r = 2r_0$ and $z = 0$ for (a) M31, (b) M31h0, (c) M31h13 and (d) M31h2: — full spectra, and for modes — $n_\theta = 0$, — $n_\theta = 1$.

mately 1 dB for M31h13 and M31h2, 3 dB for M31h3 and 4 dB for M31h4. As the hole is larger, the interactions between the jet and the plate are weaker, causing lower upstream acoustic levels. Downstream of the plate, the OASPL of the impinging jets are lower than for the free jet, which can be explained by the shielding of the acoustic radiation by the plate. This hypothesis is also supported by the fact that the levels are the lowest for the plate with the smallest hole and that they grow with the hole diameter.

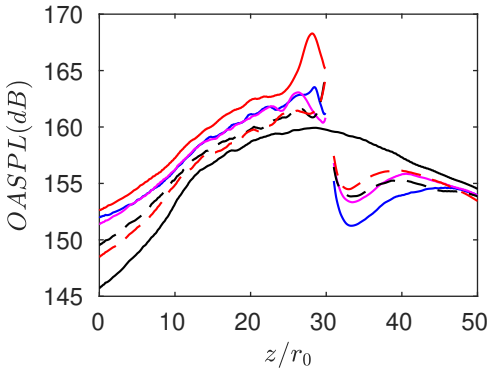

Figure 7. Variations of the OASPL at $r = 15r_0$ for — M31, — M31h0, — M31h13, — M31h2, - - - M31h3 and - - - M31h4.

5.4 Fourier decomposition of the pressure fields

A spatial Fourier transform in the radial and axial directions is applied to the pressure fields of the six jets, following the method developped by Nonomura *et al.* [16] for free jets at an exit Mach number of 2. It is applied to an area extending from $r = 5r_0$ to $r = 15r_0$ radially and from $z = 5r_0$ to $z = 25r_0$ axially. This area is chosen far enough from the jet to avoid hydrodynamic fluctuations of pressure. The amplitude thus obtained are presented in Fig. 8 as a function of the radial and axial wavenumbers k_r and k_z. For the free jet in Fig. 8(a), lobes are observed in the quadrants where k_r and k_z have the same sign, indicating they are associated with downstream propagating waves. Those lobes are aligned with the direction of propagation of the Mach waves, showing that the main acoustic component of the pressure field is linked to these waves. Similar lobes are present in the amplitude fields of the impinging jets, in Fig. 8(b) to 8(f). The same alignment of the lobes with the propagation direction of the Mach waves is noticed. However, the amplitude fields also contain lobes in quadrants with k_r and k_z of opposite sign, corresponding to upstream propagating waves. The orientation of the lobes is compared with the propagation direction of reflected Mach waves, assuming their reflection on the plate is specular. The lobes are not centered in this direction, implying the reflections of Mach waves are negligible in this case. This suggests that the main component of the upstream acoustic waves is produced by the impingement of turbulent structures on the plate. Moreover, the size of the lobes in the quadrants with k_r and k_z of opposite signs is reduced as the hole diameter increases, supporting the idea that the dominant noise component is generated by the impingement of turbulent structures on the plate.

6. CONCLUSION

In this work, one jet impinging on a plate with no hole and four jets impinging on a plate with a hole have been

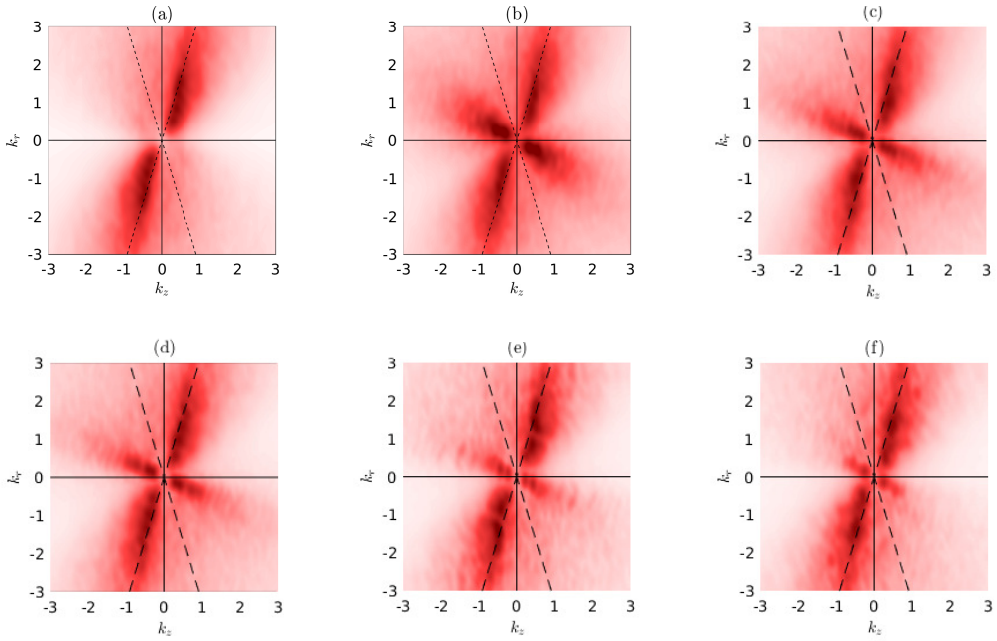

Figure 8. Amplitude fields of acoustic waves in the wavenumber (k_r, k_z) plane for (a) M31, (b) M31h0, (c) M31h13, (d) M31h2, (e) M31h3 and (f) M31h4; - - - propagation directions of incident and reflected Mach waves.

simulated in order to study the noise generated in the upstream direction. They have been compared with the corresponding free jet. The upstream acoustic levels are reduced when the hole diameter increases, which suggests that the impingement noise is the main contribution to the noise in the upstream direction. A spatial Fourier transform has been applied to the pressure fields to determine the directivity of the upstream acoustic waves. This directivity differs from the one of the reflected Mach waves, supporting that the impingement noise is dominant in the upstream direction.

7. ACKNOWLEDGMENTS

This work was financed by ArianeGroup and the DGA (Direction Générale de l'Armement). It was granted access to the HPC resources of FLMSN (Fédération Lyonnaise de Modélisation et Sciences Numériques), partner of EQUIPEX EQUIP@MESO, and of the resources of IDRIS (Institut du Développement et des Ressources en Informatique Scientifique) under the allocation 2019-2a0204 made by GENCI (Grand Equipement National de Calcul Intensif). It was performed within the framework of the Labex CeLyA of Université de Lyon, operated by the French National Research Agency (grant no. ANR-10-LABX-0060/ANR-16-IDEX-0005).

8. REFERENCES

[1] S. Kawai, S. Tsutsumi, R. Takaki, and K. Fujii, "Computational aeroacoustic analysis of overexpanded supersonic jet impingement on a flat plate with/without hole," in *ASME/JSME 2007 5th Joint Fluids Engineering Conference*, pp. 1163–1167, American Society of Mechanical Engineers, 2007.

[2] S. Tsutsumi, R. Takaki, H. Ikaida, and K. Terashima, "Numerical aeroacoustics analysis of a scaled solid jet impinging on flat plate with exhaust hole," *30th International Symposium on Space Technology and Science*, 2015.

[3] J. N. Troyes, F. Vuillot, A. Langenais, and H. Lambaré, "Coupled cfd-caa simulation of the noise generated by a hot supersonic jet impinging on a flat plate with exhaust hole," *AIAA Paper 2019-2752*, 2019.

[4] C. Bogey, O. Marsden, and C. Bailly, "Large-eddy simulation of the flow and acoustic fields of a reynolds number 10 5 subsonic jet with tripped exit boundary layers," *Physics of Fluids*, vol. 23, no. 3, p. 035104, 2011.

[5] J. Berland, C. Bogey, O. Marsden, and C. Bailly, "High-order, low dispersive and low dissipative explicit schemes for multiple-scale and boundary problems," *Journal of Computational Physics*, vol. 224, no. 2, pp. 637–662, 2007.

[6] C. Bogey and C. Bailly, "A family of low dispersive and low dissipative explicit schemes for flow and noise computations," *Journal of Computational Physics*, vol. 194, no. 1, pp. 194–214, 2004.

[7] C. Bogey, N. De Cacqueray, and C. Bailly, "A shock-capturing methodology based on adaptative spatial filtering for high-order non-linear computations," *Journal of Computational Physics*, vol. 228, no. 5, pp. 1447–1465, 2009.

[8] C. Tam and Z. Dong, "Radiation and outflow boundary conditions for direct computation of acoustic and flow disturbances in a non uniform mean flow," *Journal of Computational Acoustics*, vol. 4, no. 02, pp. 175–201, 1996.

[9] C. Bogey and C. Bailly, "Three-dimensional non-reflective boundary conditions for acoustic simulations: far-field formulation and validation test cases," *Acta Acustica united with Acustica*, vol. 88, no. 4, pp. 463–471, 2002.

[10] K. Mohseni and T. Colonius, "Numerical treatment of polar coordinate singularities," *Journal of Computational Physics*, vol. 157, no. 2, pp. 787–795, 2000.

[11] C. Bogey, N. De Cacqueray, and C. Bailly, "Finite differences for coarse azimuthal discretization and for reduction of effective resolution near origin of cylindrical flow equations," *Journal of Computational Physics*, vol. 230, no. 4, pp. 1134–1146, 2011.

[12] M. Varé and C. Bogey, "Large-eddy simulations of round jets at a mach number of 0.9 impinging on a plate with and without a hole," in *AIAA AVIATION 2020 FORUM*, p. 2549, 2020.

[13] P. Pineau and C. Bogey, "Study of the generation of shock waves by high-speed jets using conditional averaging," *AIAA Paper 2018-3305*, 2018.

[14] N. De Cacqueray, C. Bogey, and C. Bailly, "Investigation of a high-mach-number overexpanded jet using large-eddy simulation," *AIAA journal*, vol. 49, no. 10, pp. 2171–2182, 2011.

[15] M. Harper-Bourne, "The noise from shock waves in supersonic jets-noise mechanism," *Agard Cp-131*, 1974.

[16] T. Nonomura, H. Nakano, Y. Ozawa, D. Terakado, M. Yamamoto, K. Fujii, and A. Oyama, "Large eddy simulation of acoustic waves generated from a hot supersonic jet," *Shock Waves*, pp. 1–22, 2019.